ELSEVIER

Journal of Wind Engineering
and Industrial Aerodynamics 89 (2001) 569–598

JOURNAL OF wind engineering AND industrial aerodynamics

www.elsevier.com/locate/jweia

The applicability of quasi-steady theory to pressure statistics beneath roof-top vortices

D. Banks[a,*], R.N. Meroney[b]

[a] *Cermak Peterka Petersen, 1415 Blue Spruce Drive, Fort Collins, CO 80524, USA*
[b] *Fluid Mechanics and Wind Engineering Program, Civil Engineering Department, Colorado State University, Fort Collins, CO 80523, USA*

Abstract

During cornering winds, dual conical vortices form in the separated flow along the leading edges of flat roofs. These vortices cause the most extreme wind induced suction forces found anywhere on the building, so it is important to predict them accurately. The quasi-steady theory is commonly used to predict building surface pressures using upstream flow conditions. However, many studies have concluded that the quasi-steady theory should not be used in the separated flow regions of a building, because it underpredicts the peak and rms pressure coefficients, C_{p^v} and $C_{p_{\rm rms}}$. A wind tunnel study of a low-rise building is performed to examine why C_{p^v} and $C_{p_{\rm rms}}$ are underpredicted. The study uses simultaneous pressure and velocity measurement to assess the basic assumption of quasi-steady theory in this situation, which is that an instantaneous change in wind direction (ω) will have the same effect on vortex position and strength as a long-term change in ω. This assumption is found to be valid only for wind angles of $45^\circ \pm 10^\circ$, and primarily for low-frequency changes in ω. This ought to actually result in an overprediction of C_{p^v} and $C_{p_{\rm rms}}$, as quasi-steady theory is shown to overestimate the effects of vortex motion due to lateral turbulence. However, the quasi-steady theory ignores the contributions to C_{p^v} and $C_{p_{\rm rms}}$ from random vortex motion and random changes in vortex strength. The authors apply an analytical model of the vortex flow that links vortex behaviour to surface pressure to assess these contributions, and show that their absence results in the net underprediction of C_{p^v} and $C_{p_{\rm rms}}$, even when the quasi-steady theory is applied fully, with no linear simplifications.

*Corresponding author. Tel.: +1-970-221-3371; fax: +1-970-221-3124.
E-mail address: dbanks@cppwind.com (D. Banks).

0167-6105/01/$ - see front matter
PII: S0167-6105(00)00092-1

CEP 99-00-7

Nomenclature

B	largest building plan dimension (either length or width)
C_p	pressure coefficient $= (p - p_{\text{ref}})/\frac{1}{2}\rho U_{\text{ref}}^2$
C_{p_S}	C_p at the point S (The point S moves in time along on the roof surface, tracking directly beneath the moving vortex core. $C_{p_S}(t)$ is measured at a given x as the minimum of the concurrently measured $C_{p_{\text{tap}}}(t)$ values for a row of taps normal to the roof edge)
$C_{p_{\text{tap}}}$	C_p at a given fixed tap location
$C_p^{\text{nom}\theta}$	mean C_p as a function of the nominal wind angle
$C_p^{\text{inst}\theta}$	mean C_p as a function of the instantaneous wind angle, calculated from $C_p^{\text{nom}\theta}$
$C_{\bar{p}_{\text{meas}}}^{\text{inst}\theta}$	mean C_p as a function of the instantaneous wind angle, measured experimentally
$C_{\bar{p}}$, $C_{p^\vee}$	mean, and peak negative values of the pressure coefficient time series $C_p(t)$, where $C_p(t) = (p(t) - p_{\text{ref}}(t))/\frac{1}{2}\rho U_{\text{ref}}^2)$
$C_{p_{mean}}$, $C_{p_{\text{rms}}}$	mean and rms values of pressure coefficient time series
$C_{p_{\text{rms}}\_\text{TI}}$	component of $C_{p_{\text{rms}}}$ due to turbulence intensity
$C_{p_{\text{rms}}\_\text{X}}$	component of $C_{p_{\text{rms}}}$ due to variable 'X', where X is one of θ', and ω'
f	frequency
$f_x(x)$	probability distribution function (pdf) for the variable 'x'
G	gust factor
g	integral of centripetal acceleration from inviscid region, through core, to roof
H	height of building
I_U	turbulence intensity in the longitudinal (along wind) direction
k	ratio of velocities (constant)
p	static pressure
q	flow head$(= \frac{1}{2}\rho U^2)$
R	dummy variable
t	time
U	flow speed
U_{ref}	flow speed measured upstream at roof height
$U_{(\text{point})}$	U at the location (point) ex: U_C, U_M
x	distance from the apex or leading edge corner, measured along the leading edge
y	distance from the leading edge wall, along a line normal to the leading edge
z	distance above the roof surface
α	wind angle above the vortex, relative to the vortex core axis
ϕ	angle formed along the roof surface with respect to the leading edge

ϕ_c	angle formed between the ray of the vortex core position and the leading edge
η	transfer function to calculate C_p at a fixed tap based on tap location and C_{ps}.
θ	horizontal wind direction relative to the entire building (0–360° scale)
ρ	air density
σ_x	standard deviation of quantity represented by the variable x (ex: U, C_p)
ω	wind angle relative to a given edge and corner (90° is normal to the edge)
ω'	normalized fluctuations in the virtual or effective wind angle, $\omega'(t) = [\omega^{\text{virtual}} - \omega(t)] \div \omega(t)$
ω_{nom}	nominal wind direction, determined by the orientation of the model building
ξ	dummy variable

Subscripts generally denote the position in space at which a quantity is measured, i.e., C_{ps} is the pressure coefficient at the point S, which is directly beneath the center of the moving vortex core.

Overbars indicate time averaged quantities (ex: $\bar{g}$).

Prime symbols indicate fluctuating quantities (ex: g').

1. Introduction

The quasi-steady theory is a simple, practical model which links a building's surface pressure fluctuations directly to fluctuations in the local wind vector. The accuracy of the quasi-steady theory is important because it is the assumption embodied in many building codes [1], where the design pressure is calculated using an equation of the form

$$p = q_z G C_p, \tag{1}$$

where q_z is the flow head at height $z = \frac{1}{2}\rho(\bar{U}_z)^2$, G the expected gust factor, C_p the mean pressure coefficient.

The C_p values are generally measured through wind tunnel studies, and the results are tabulated for various building types and atmospheric boundary layer conditions. If Eq. (1) is valid, then knowledge of the velocity time series at the roof height on the location where a building is to be constructed allows a prediction of the loads on the roof once the building is in place.

On buildings with flat roofs and sharp roof/wall edges, flow separation occurs along the roof edge. This separation may take on two forms. For flow $\pm 20°$ about the normal to the roof edge, a condition called bubble separation dominates. In this situation, there is high suction between the roof edge and the point of reattachment. Peak suctions are generated when cylindrical vortices are formed along the roof edge

and are convected through the separated flow zone towards the re-attachment point [2]. For flow $\pm 25^\circ$ from a cornering flow, dual conical vortices exist. These are responsible for the largest suctions on the rooftop.

Unfortunately, many studies have concluded that the quasi-steady theory fails to adequately predict pressures in separated flow, and in particular beneath or near the conical vortices [3–6].

1.1. Review of quasi-steady theory

The quasi-steady equation can be derived from two assumptions:

(1) The flow field is steady, inviscid, irrotational, and incompressible, and so obeys the Bernoulli equation, given by

$$\tfrac{1}{2}\rho U_{\mathrm{ref}}^2(t) + p_{\mathrm{ref}}^{\mathrm{static}}(t) = \tfrac{1}{2}\rho U_{\mathrm{M}}^2(t) + p_{\mathrm{M}}^{\mathrm{static}}(t),$$

where the subscript ref indicates the position of reference measurement (usually upstream and to the side of the model), and the subscript M indicates a suitable measurement position anywhere in the flow field.

(2) The steady condition can be extended to a quasi-steady regime where the entire flow field velocity changes simultaneously if the flow is Reynolds number independent, or $U_{\mathrm{M}}(t) = kU_{\mathrm{ref}}(t)$, where k is the constant.

Finally the pressure coefficient C_p is defined as

$$C_p(t) \equiv \frac{p_{\mathrm{M}}^{\mathrm{static}} - p_{\mathrm{ref}}^{\mathrm{static}}(t)}{\tfrac{1}{2}\rho(\overline{U_{\mathrm{ref}}})^2}.$$

Combining these three equations at the point M gives

$$C_{p_{\mathrm{M}}}(t) = \frac{U_{\mathrm{ref}}^2(t) - U_{\mathrm{M}}^2(t)}{(\overline{U_{\mathrm{ref}}})^2} = \left(\frac{U_{\mathrm{ref}}(t)}{\overline{U_{\mathrm{ref}}}}\right)^2 (1 - k^2). \tag{2a}$$

Time averaging $C_{p_{\mathrm{M}}}(t)$ gives $C_{\bar{p}_{\mathrm{M}}} = \overline{C_{p_{\mathrm{M}}}(t)} = (1 + I_U^2)(1 - k^2)$, since $\overline{(U(t)/\bar{U})^2} = 1 + I_{\mathrm{U}}^2$; hence

$$C_{p_{\mathrm{M}}}(t) = \left(\frac{U_{\mathrm{ref}}(t)}{\overline{U_{\mathrm{ref}}}}\right)^2 \frac{C_{\bar{p}_{\mathrm{M}}}}{1 + I_U^2}. \tag{2b}$$

Here, a third assumption is introduced: If the value of $C_{\bar{p}_{\mathrm{M}}}$ is dependent upon wind direction, a function $C_{\bar{p}_{\mathrm{M}}}(\theta)$ can be used. This implies that the expected value of $C_{p_{\mathrm{M}}}(t)$ is independent of the previous wind direction, the rate of change of wind direction, or the mean wind direction, and depends only on the value of $\theta(t)$ at that instant.

The turbulence intensity term, I_U^2, is often neglected. Assuming that this relationship applies to $p_{\mathrm{M}}^{\mathrm{static}}$ measured on the surface of a building, one obtains the quasi-steady expression often used in wind engineering:

$$Cp^{\mathrm{Q-S}}(t) = \left(\frac{U_{\mathrm{ref}}(t)}{\bar{U}_{\mathrm{ref}}}\right)^2 C_{\bar{p}}(\theta_{\mathrm{ref}}(t)). \tag{3}$$

The function $C_{\bar{p}}(\theta)$ that is used in Eq. (3) is typically produced from wind tunnel studies in which the model building is rotated through 360° at 5° or 10° increments. The mean pressure coefficient $\left(\overline{C_p(t)}\right)$ is calculated for each rotation position, and this is tabulated as the $C_{\bar{p}}(\theta)$ value for the corresponding wind direction. Once compiled, these values produce the $C_{p_{\text{mean}}}(\theta)$ or $C_{\bar{p}}(\theta)$ plot typically reported in wind engineering literature. In this paper, I will refer to this function as the mean value of $C_p(t)$ for a nominal wind direction of θ, or $C_{\bar{p}}^{\text{nom}\theta}(\theta)$. As Richards has demonstrated [7], $C_{\bar{p}}^{\text{nom}\theta}(\bar{\theta})$ is not theoretically the same as the value of $\overline{C_p(t)}$ when the wind direction has an instantaneous value of $\theta(t) = \bar{\theta}$. This latter function will be referred to in this paper as $C_{\bar{p}}^{\text{inst}\theta}(\bar{\theta})$. As will be shown in Section 4.1, where $C_{\bar{p}}^{\text{nom}\theta}(\bar{\theta})$ is calculated from $C_{\bar{p}}^{\text{inst}\theta}(\bar{\theta})$, $C_{\bar{p}}^{\text{nom}\theta}$ has lower peaks than $C_{\bar{p}}^{\text{inst}\theta}(\bar{\theta})$. Since the quasi-steady theory purports to estimate the effects of instantaneous wind direction change, $C_{\bar{p}}^{\text{inst}\theta}(\bar{\theta})$ is a more correct function for use in Eq. (3) than $C_{\bar{p}}^{\text{nom}\theta}(\bar{\theta})$.

2. Experimental methods

2.1. Experimental design

The first quasi-steady assumption implies that at a building tap, the surface pressure coefficient, $C_{p_{\text{tap}}}$, is a function solely and directly of the velocity of the flow passing immediately over that tap, U_{tap}. The second quasi-steady assumption, that $U_{\text{tap}}(t) = kU_{\text{ref}}(t)$, implies that the correlation between U_{tap} and a reference velocity measured anywhere else in the flow field is 1.0. When these two implications are combined, quasi-steady theory is seen to predict a cross correlation of 1.0 between $C_{p_{\text{tap}}}(t)$ and $U_{\text{ref}}(t)$.

Measurements show that the actual cross correlations are much lower [5], and that the correlation between $C_{p_{\text{tap}}}$ and upstream flow velocity drops very quickly as the distance between the reference location and the building is increased [8]. This is at least in part because the correlation between any two points in the turbulent boundary layer flow drops as the distance between them increases. This means that for Eq. (3) to be strictly correct, U_{ref} and θ_{ref} must be measured directly above the tap, and the validation amounts to a confirmation of Bernoulli's theorem.

This loss of correlation between U_{ref} and U_{tap} does not preclude the use of quasi-steady theory for all but this trivial case, however. The objective of quasi-steady theory is to allow pressure statistics such as mean C_p, $C_{p_{\text{rms}}}$ (σ_{C_p}), the probability distribution function (pdf) and the power spectrum of $C_p^{\text{Q-S}}(t)$ to be assessed from the local wind statistics and a general knowledge of $C_{\bar{p}}(\bar{\theta})$. As long as θ_{tap} and the normalized U_{tap} have similar statistical properties to θ_{ref} and the normalized U_{ref}, then Eq. (3) should accurately predict these pressure statistics. In cases where Eq. (3) fails to do so, it is often assumed that this is because the building has altered the nature of the flow passing around it in such a way that the statistics of θ_{tap} and U_{tap} no longer match those of as θ_{ref} and U_{ref}. This is often referred to as "building interference".

In the case of taps near the conical vortices, measurements indicate that the statistics of velocities measured directly above the taps are indeed substantially different from those of the undisturbed upstream flow, exhibiting a much greater turbulence intensity, as well as flow reversals [9]. However, the correlation between these U_{tap} measurements and $C_{p_{\text{tap}}}$ are quite low (less than 0.5) because $C_{p_{\text{tap}}}$ is controlled not by the immediate U_{tap} velocity, but rather by the proximity and strength of the vortex. The location and strength of the vortex, in turn, are controlled in large part by the speed and direction of flow above the vortex. The nature of this control will be briefly described in the following section, but for now it is worth noting that this assessment is corroborated by the high cross correlation (above 0.8) between the flow velocity measured at a point M directly above the core and the suction at a point S directly beneath it. These points are depicted in Fig. 1, along with some of the nomenclature used in this report.

In addition, as shown in Fig. 2, the flow velocity and direction statistics above the vortex provide a very good match to those of the undisturbed upstream reference flow. To the extent that U_{M} and θ_{M} control the vortex, then, one would therefore expect the quasi-steady theory to do a reasonably good job of predicting pressure statistics under the vortex. To understand how and why this is not generally the case, this study experimentally measures the validity of the immediate quasi-steady

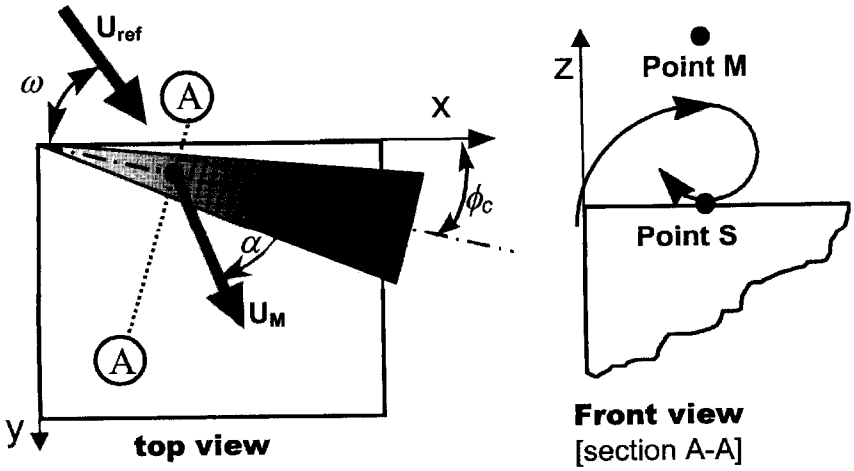

- Single conical vortex shown as shaded triangle (Second vortex not shown)
- Dashed line indicates the position of the vortex core's axis
- ω = wind angle of reference wind relative to the roof's leading edge
- α = wind angle relative to vortex core axis at the point M
- ϕ_c = vortex core angle with respect to the roof's leading edge
- the point S is on the roof surface directly beneath the vortex core
- the point M is above the shear layer, directly above the vortex core

Fig. 1. Nomenclature for model of vortex mechanism.

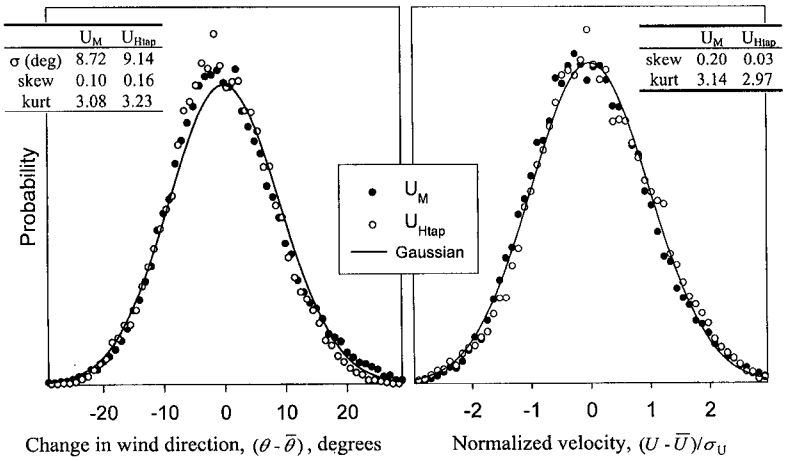

Fig. 2. Probability distributions, with skewness and kurtosis, for: (●) $U_M(t)$: Wind vector directly above the vortex core. (○) $U_{H_{tap}}$: wind vector at roof height when building model has been removed from the tunnel.

relationship,

$$C_p^{Q-S}(t) = \left(\frac{U_M(t)}{\bar{U}_M}\right)^2 C_{\bar{p}}(\theta_M(t)), \tag{4}$$

using concurrent measurement of $C_p(t)$, $U_M(t)$ and $\theta_M(t)$.

2.2. Model scale tests

As noted above, the location of the vortex is an essential parameter for determining the expected suction at any given pressure tap near the vortex. Simultaneous flow visualization and pressure measurement show that the peak suction always appears beneath the moving vortex core [10], so $\phi_C(t)$ can be measured using a row of simultaneously sampled pressure taps normal to the roof edge. Several such rows were drilled in a 1 : 50 model of the TTU WERFL field site [11] (see Fig. 3). The model was placed in the CSU B2 turbulent atmospheric boundary layer developed by Ham [12]. This boundary layer features a power law exponent of 0.14 with turbulent intensities at roof height of 19% (along wind) and 15% (lateral).

Pressures at all 48 taps were measured sequentially at 23809 Hz, for a per-tap return frequency of 496 Hz, using a Pressure Systems Inc. (PSI) ESP48 transducer unit mounted inside the model. A restrictor tubing system with a flat response (Gain = 1.00 ± 0.05, linear phase) out to 200 Hz was used for pressure measurements. The tap diameter was 0.5 mm.

Horizontal (x and y) velocities were simultaneously measured, also at 496 Hz, using a Thermal Systems Inc. (TSI) model 1241 x-wire hot-film probe connected to a 1050 constant temperature anemometer. The probe was positioned at a point M

row #1: x=30mm		
tap#	y,mm	ϕtap
9	8	14.9
10	11	20.1
11	14	25.0
row #2 x=60mm		
tap#	y,mm	ϕtap
12	8	7.6
13	11	10.4
14	14	13.1
15	17	15.8
16	20	18.4
17	25	22.6
18	30	26.6
row #3: x=87mm		
tap#	y,mm	ϕtap
38	5	3.3
39	10	6.6
40	15	9.8
41	20	12.9
42	25	16.0
43	30	19.0
44	35	21.9
45	45	27.3
46	55	32.3
47	65	36.8
48	85	44.3

row #4: x=112mm		
tap#	y,mm	ϕtap
32	5	2.6
33	10	5.1
34	15	7.6
35	20	10.1
36	25	12.6
37	30	15.0
row #5: x=137mm		
tap#	y,mm	ϕtap
19	5	2.1
20	10	4.2
21	15	6.2
22	20	8.3
23	25	10.3
24	30	12.4
25	35	14.3
26	45	18.2
27	55	21.9
28	65	25.4
29	85	31.8
30	135	44.6
31	175	51.9

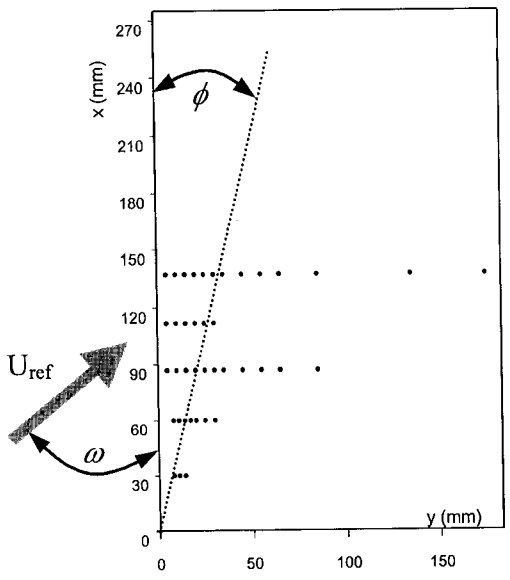

Fig. 3. Top view of 1 : 50 model of TTU WERFL building showing position and numbering of roof-top pressure taps used in this experiment.

located above the shear layer. A typical location for many of the measurements presented in this paper was 16 mm directly above tap #40, but the probe was also placed above other taps.

A conditional sampling procedure was employed during the data analysis to isolate the effects of various parameters. For example, to eliminate the effects of vortex motion on the mean values of U_M or the $C_p(\phi)$ profile, only those velocities or pressures measured when a target tap measured the minimum C_p for row #3 would be included in the statistics. (This procedure was employed in generating the data for Figs. 2 and 5.) Another example used in this study is to calculate statistics using only those $C_p(t)$ or $\phi_C(t)$ values measured when $\omega(t)$ was within a certain range (Fig. 6). The conditional sampling technique is detailed in Ref. [13].

3. The vortex flow mechanism model

As mentioned above, the pressure coefficient beneath the vortex core is a function of the vortex strength, as well as the wind speed and wind direction above the vortex. Banks and Meroney have studied this relationship and developed the following expression for the surface pressure coefficient directly beneath the moving vortex core [13,14]:

$$C_{ps}(t) = \left(\frac{U_M(t)}{\bar{U}_M(\omega)}\right)^2 \left[1 - \left(\frac{\bar{U}_M(\omega)}{\bar{U}_{ref}}\right)^2 \left(1 + \sin^2(\alpha(t))g(\omega(t), t)\right)\right], \quad (5)$$

where ω is the wind angle ($\omega = 90°$ for flow normal to the wall nearest the tap), α is the wind direction relative to the vortex core (Note that the flow direction changes by an amount $\Delta\omega \approx \phi_C$ as it passed over the roof edge, so that $\omega \approx \alpha$). U_M is the total flow speed at a measurement point above the shear layer, directly above the vortex core (selected experimentally at $z = 3.5$ times the mean core height), U_{ref} is the flow velocity at roof height upstream of the model.

Many of these terms were illustrated in Fig. 1. The term g expresses the pressure drop across the vortex core from the point M to the point S, and is an indication of the quality or strength of the vortex; $g = 0$ for no vortex, while $g \approx 1.5$ for a well formed vortex. The function g can be divided by separation of variables:

$$g(\omega(t),\ t) = \bar{g}(\omega)g'(t),$$

where $g'(t)$ is a nearly Gaussian random variable which accounts for random changes in the vortex quality, and $\bar{g}(\omega)$ decreases with increasing ω, possibly as the result of the lack of axial flow destabilizing the conical vortex. This model is developed and validated in some detail in Refs. [13,15].

3.1. Comparison of the vortex flow mechanism model with Q-S theory

Note that C_{p_S} does not correspond to the suction at a single tap, since the vortex core moves in response to changes in wind direction, as shown in Fig. 4. This complicates the comparison of Eqs. (4) and (5). However, the pressure at a single tap can be calculated from C_{p_S} if the location of the core ($\phi_c(t)$) is known. Since the mean core position is a function of the wind angle $\omega(t)$, the position of the tap relative to the core dictates $C_{p_{tap}}$ according to the equation:

$$C_{\tilde{p}_{tap}}(\omega) = \left(C_{\tilde{p}_S}(\omega) - C_{p_a}\right)\eta(\omega) + C_{p_a},$$

where C_{p_a} is the asymptotic value of $C_p(\phi)$ in the middle of the roof, beyond the influence of the vortex. The function η is explained in Fig. 5. It acts as a transfer function, using the mean $C_p(\phi)$ pressure profile shape and the location of the vortex

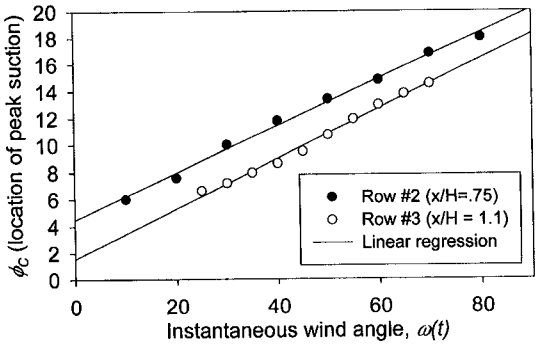

Fig. 4. Position of vortex core as a function of wind direction.

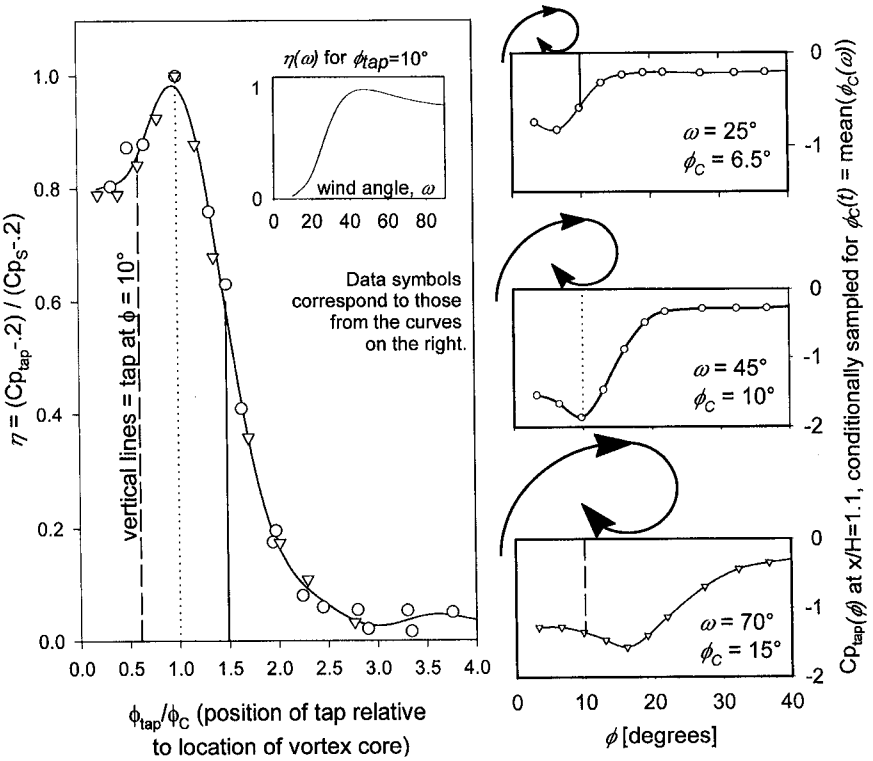

Fig. 5. Calculation of $C_p(\omega)$ at a given tap using the mean C_p profile and the location of the tap relative to the location of the vortex core for each wind direction ω.

core relative to the tap in question to convert the $C_{p_S}(\omega)$ function into a $C_{p_{tap}}(\omega)$ function.

The vortex core also moves randomly about its mean position for any given wind direction. This is illustrated in Fig. 6, where the vortex core position above tap row #2 (taps 12–18) was determined at each time step using the instantaneous location of the peak suction.

It is known that changes in turbulence intensity affect the mean reattachment position for bubble separation [16]. It has been postulated that this is the result of very high frequency turbulence (of the same scale as the shear layer) increasing entrainment between the shear layer and the separated flow zone [17]. It is possible that changes in this high frequency shear layer turbulence from one moment to the next influence the size and motion of the vortex.

Regardless of their causes them, for the purpose of this analysis, these fluctuations in vortex position are considered random, and their effects on the time dependent value of $C_{p_{tap}}$ can be incorporated in Eq. (5) through the term ω':

$$C_{p_{tap}}(t) = \left(C_{p_S}(t) - C_{p_a}\right)\eta(\omega(1+\omega')) + C_{p_a}.$$

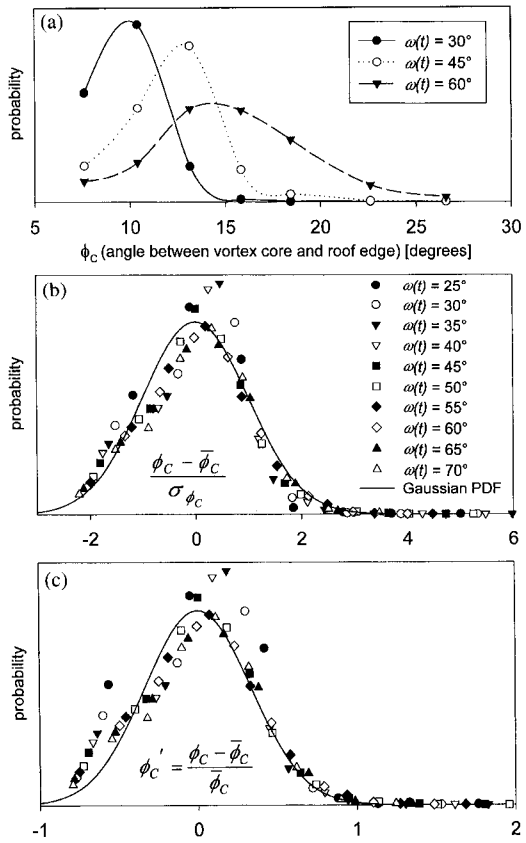

Fig. 6. (a–c) Histogram of vortex core position in tap row #3 for various instantaneous wind angles during a test with a nominal wind angle of $\omega_{\text{nom}} = 45°$. All $\omega(t)$ values are $\pm 2.5°$.

Since there is a linear relationship between $\phi_c(t)$ and $\omega(t)$, the random changes in vortex position have been expressed as random changes in a "virtual" or effective wind angle by defining

$$\omega'(t) = \frac{\omega^{\text{virtual}}(t) - \omega(t)}{\omega(t)}.$$

The pdf of ω' is very similar to that of $\phi_c'(t)$ in Fig. 6c. It is a Gaussian random variable with mean 0 and $\sigma_{\omega'} = 1/3$.

The full equation for $C_p(t)$ at a tap under the region of vortex influence in now given by

$$C_{p_{\text{tap}}}(t) = \left(\frac{U_M(t)}{\bar{U}_M(\omega)}\right)^2 C_{p_{\text{tap}}}(\omega),$$

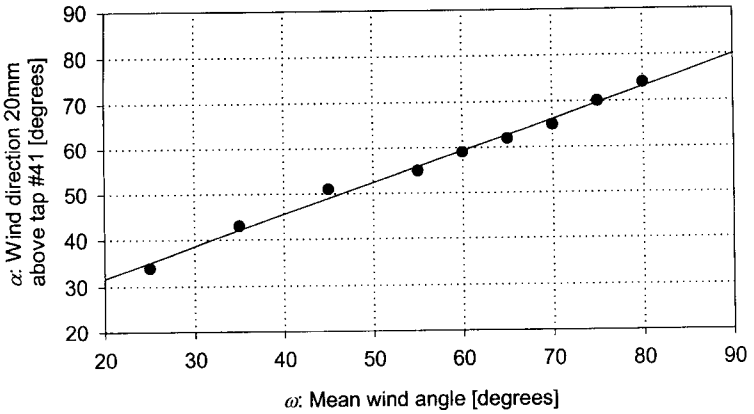

Fig. 7. The dependence of wind direction at the point M on upstream wind direction.

$$C_{p_{\text{tap}}}(\omega) = \left[1 - \left(\frac{\bar{U}_{\text{M}}(\omega)}{\bar{U}_{\text{ref}}}\right)^2 (1 + \sin^2(\alpha(t))\bar{g}(\omega(t))g'(t)) - C_{p_a}\right]\eta(\omega(1+\omega')) + C_{p_a}. \tag{6}$$

Since $\alpha(t)$ is essentially a function of $\omega(t)$ (see Fig. 7), Eq. (6) has the same form as the quasi-steady equation. The influence of the $g'(t)$ and $\omega'(t)$ terms is assessed in Section 4.2.

3.2. *Frequency considerations: coherence and spectral analysis*

The quasi-steady theory has been interpreted to imply that the coherence, cross-correlation (between taps) and spectrum of wind-induced pressures should be equal to those of the local wind velocity head. This has been shown to be invalid, as the pressure spectra attenuate faster than the velocity spectra [18,19], and the local pressure coherence and cross-correlation under the separated flow zones are greater than that of the incident flow [20].

The increased cross-correlation is the result of the existence of a coherent flow structure (the conical vortex), which is not in the upstream flow. This is an essential consideration when calculating total loads. This aspect of what is sometimes considered "building interference" will not be directly addressed in this paper, other than the qualitative discussion which follows here.

Calculating the pressure spectrum from that of the incident flow has been addressed successfully for taps on the windward wall through the use of an admittance function, which cuts off the incident flow turbulence at $fB/U \approx 0.2$, or gusts roughly five times the largest building plan dimension (B) [21]. The flow mechanism described in Refs. [13–15] and embodied in Eq. (6) suggests that a similar

admittance can be used to describe the relationship between upstream flow and roof pressures beneath the conical vortices.

In the vortex flow mechanism model, the vortex can be seen as a wheel being spun by the flow passing over it. Through the term g, this spinning amplifies the pressure drop associated with a given wind gust above the vortex, so that the pressure drop at the surface is more severe than that due simply to the additional flow speed. As a result, while all gusts can be expected to directly influence the surface pressure through the $U_M(t)/\text{mean}(U_M)$ term, only those gusts large enough to spin the vortex faster ($fB/U<10$) would be fully "amplified" at C_{ps}. The size of gust needed decreases as the vortex gets smaller near the apex of the roof, so the admittance would be a function of x.

Only lateral gusts (i.e., changes in $\omega(t)$) that are larger than the building ($fB/U<1$) would be expected to move the vortices, causing them to "sway" from side to side. Since an increase in ω for one conical vortex implies a decrease in ω for the other, and C_{ps} increases as $\omega(t)$ approaches 60°, the vortex sway will also produce low frequency suction fluctuations which are correlated to low frequency upstream lateral turbulence. This has been observed through simultaneous pressure measurement over the whole roof surface [22]. For many taps, especially those that are intermittently under the vortex and in the re-attachment zone, the vortex core position (as expressed by the $\eta(\omega)$ term) is the dominant influence on surface pressure. As a result, these taps will exhibit a strong correlation in suction with the lower frequency lateral turbulence that causes the mean vortex position to change.

The notion of an admittance is fundamental to the validation of the quasi-steady theory; it is clear that for low enough frequencies, the quasi-steady theory will hold true. For example, a wind direction change lasting over a minute at full scale ($fB/U \approx 0.03$) ought to have the same effect as a shift in mean wind direction, while a gust with $fB/U = 10$ would not be expected to affect the mean flow pattern around the building in any significant way. As long as gusts which are of sufficient size and duration to affect a structural element of interest are passed on to the building surface pressure in keeping with Eq. (3), then the quasi-steady model is, for practical purposes, valid for point pressures. In this context, the question is not so much one of the validity of the quasi-steady model, but rather one of its frequency limits. For this reason, the effects of data filtering will be addressed in Section 4.1.

4. Discussion of results

4.1. Part 1: mean pressures

As noted in the introduction and in Ref. [7], the expected value of $C_p(t)$ when the wind instantaneously comes from an angle θ_0, which is calculated as

$$C_{\bar{p}}^{\text{inst}\theta}(\theta_0) = \overline{C_p(t)} \quad \text{when } \theta(t) = \theta_0,$$

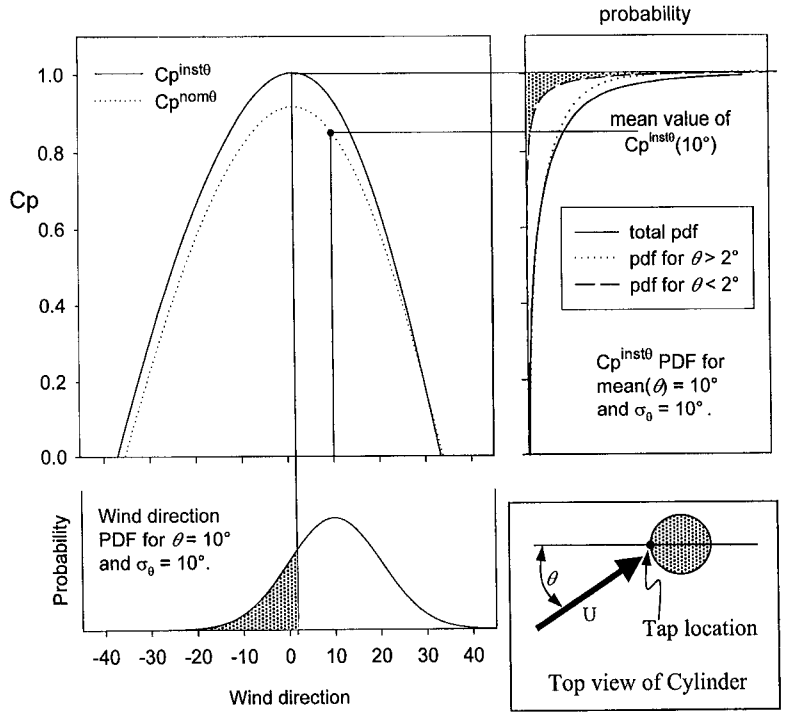

Fig. 8. Graphical illustration of the relationship between the $C_{\bar{p}}^{\text{inst}\theta}$ and $C_{\bar{p}}^{\text{nom}\theta}$ curves and the $\theta(t)$ and $C_p^{\text{inst}\theta}(t)$ probability distribution functions, for the case of $\bar{\theta} = 10°$.

is not the same as the measured or expected value of $C_p(t)$ for a nominal or run-averaged wind direction of $\bar{\theta}$, which is calculated as

$$C_{\bar{p}}^{\text{nom}\theta}(\theta_0) = \overline{C_p(t)} \quad \text{when } \overline{\theta(t)} = \theta_0.$$

The expected value of $C_{\bar{p}}^{\text{nom}\theta}(\theta)$for a given wind direction θ_0 can be calculated from $C_{\bar{p}}^{\text{inst}\theta}(\theta)$; since the wind direction has a Gaussian distribution,

$$C_{\bar{p}}^{\text{nom}\theta}(\theta_0) = \frac{1}{\sqrt{2\pi}\sigma_\theta} \int_{-\infty}^{\infty} C_{\bar{p}}^{\text{inst}\theta}(\theta) \exp(-(\theta - \theta_0)/2\sigma_\theta)^2 \, \mathrm{d}\theta. \tag{7}$$

Since $C_{\bar{p}}^{\text{nom}\theta}(\theta)$ is known, Eq. (7) was solved by assuming a $C_{\bar{p}}^{\text{inst}\theta}(\theta)$ function and iteratively improving this assumption by minimizing the residual.[1]

The distribution of $\theta(t)$ causes $C_{\bar{p}}^{\text{inst}\theta}(\theta)$ to be averaged over a range of wind angles when calculating $C_{\bar{p}}^{\text{nom}\theta}(\theta_0)$. This is illustrated in Fig. 8 for data on the front face of a circular cylinder, where the $C_{\bar{p}}^{\text{nom}\theta}(\theta_0)$ curve was adapted from data in Ref. [24]. If the mean wind direction is 10°, then the probability that $C_p(t) = 1.0$ is directly

[1] Note that Papoulis [23] shows that a relationship such as that expressed in Eq. (7) can be approximated as $C_{\bar{p}}^{\text{inst}\theta}(\theta) \approx C_{\bar{p}}^{\text{nom}\theta}(\theta) - (\mathrm{d}^2 C_{\bar{p}}^{\text{nom}\theta}(\theta)/\mathrm{d}\theta^2)(\sigma_\theta^2/2)$, which in the case of Fig. 8 agrees quite well with the full iterative solution to Eq. (7). This approximation has proven much less accurate for $C_p(\theta)$ under a vortex.

related to the probability that $\theta = 2°$, and the probability that $C_p(t) = 0.2$ is related to the probability that $\theta = 30°$. The net result of combining the $\theta(t)$ pdf for $\bar{\theta} = 10°$ with the $C_{\bar{p}}^{\text{inst}\theta}(\theta)$ curve is the negative exponential $C_p^{\text{nom}\theta}$ pdf shown in the upper right corner of Fig. 8, where the shaded region of the $C_p^{\text{nom}\theta}$ pdf corresponds to the shaded region of the $\theta(t)$ pdf. Section 4.3 provides more details on the calculation of this type of $C_p^{\text{nom}\theta}$ pdf, but for now we will simply note that the mean or expected value of this $C_p^{\text{nom}\theta}$ pdf gives $C_{\bar{p}}^{\text{nom}\theta}$ (10°).

We see from this procedure that the value of $C_{\bar{p}}^{\text{nom}\theta}$ (2°) is a weighted average of the surrounding $C_{\bar{p}}^{\text{inst}\theta}(\theta)$ values, which must be less than $C_{\bar{p}}^{\text{inst}\theta}$ (2°), since this is a peak value. In general, $|C_{\bar{p}}^{\text{nom}\theta}(\bar{\theta})|$ will be less than $|C_{\bar{p}}^{\text{inst}\theta}(\theta)|$ for peak values.

The underlying assumption for this type of calculation is that a universal function $|C_{\bar{p}}^{\text{inst}\theta}(\theta)|$ exists for this tap; or that regardless of the nominal wind direction $\bar{\theta}$, an instantaneous shift in wind direction to θ will produce the same surface pressure at that tap. This assumption has been tested at CSU using data from the experimental configuration described in Section 2, where $\theta(t)$ is measured at the point M. Fig. 9 shows data from tests where the x-wire was placed 24 mm above tap #41. This point is about 3 times as far above the surface as the expected vortex core height at $\omega = 45°$, and is out of the separated flow, above the shear layer.

Each plot includes two $C_{\bar{p}}^{\text{inst}\theta}$ curves, calculated above from Eq. (7) using $\sigma_\omega = 8°$ and $\sigma_\omega = 10°$, and the $C_{\bar{p}}^{\text{nom}\theta}$ curve for tap #9 from which they are derived. These curves illustrate again how $|C_{\bar{p}}^{\text{inst}\theta}| > |C_{\bar{p}}^{\text{nom}\theta}|$ at pressure peaks like those at $\omega = 20°$ and $\omega = 60°$. Each individual plot shows the measured $C_{\bar{p}}^{\text{inst}\theta}(\omega)$ values for the given nominal wind angle $(C_{\bar{p}_{\text{meas}}}^{\text{inst}\theta}(\omega(t), \omega_{\text{nom}}))$. The simultaneously recorded $C_p(t)$ and $\omega(t)$ time series were sorted by ω, and successive groups of 500 data points were averaged for each filled circle data point. This procedure was repeated after the C_p and ω time series were filtered at 2 Hz (5th order Butterworth filter) to produce the open circle data points. The measured σ_ω for the unfiltered and filtered $\omega(t)$ time series was 10° and 8°, respectively.

While the plots for $\omega_{\text{nom}} = 15°$ and $\omega_{\text{nom}} = 25°$ confirm that the value of $C_{\bar{p}}^{\text{nom}\theta}$ does not necessarily lie on the $C_{\bar{p}}^{\text{inst}\theta}$ curve, the $C_{\bar{p}_{\text{meas}}}^{\text{inst}\theta}$ curves do not follow the predicted $C_{\bar{p}}^{\text{inst}\theta}$ values very well, especially for $\omega(t) < 15°$. This indicates that the separation bubble on the other wall, which is responsible for the secondary negative peak at $\omega = 0°$, does not establish fully when the wind momentarily shifts to $\omega(t) = 0°$.

For $\omega_{\text{nom}} = 35°$ and $\omega_{\text{nom}} = 45°$, the measured and predicted $C_{\bar{p}}^{\text{inst}\theta}$ curves show good agreement as the conical vortex moves away from the leading edge and over the tap. Quasi-steady theory assumes that $C_{\bar{p}_{\text{meas}}}^{\text{inst}\theta}$ will fall on the predicted $C_{\bar{p}}^{\text{inst}\theta}$ curve, so for these angles, quasi-steady theory can be expected to be accurate.

For $\omega_{\text{nom}} = 55°$ and $\omega_{\text{nom}} = 65°$, the unfiltered experimental data still follow the predicted $C_{\bar{p}}^{\text{inst}\theta}$ behaviour for $\omega < 60°$, but for $\omega > 60°$, these data stay at a higher suction than the predicted curve. We suspect that this is because the vortex is more likely to remain stable during a brief wind direction excursion of $\omega > 65°$ than for a longer duration wind direction change. This is confirmed by the fact that the data do follow the predicted $C_{\bar{p}}^{\text{inst}\theta}$ curves when low pass filtered.

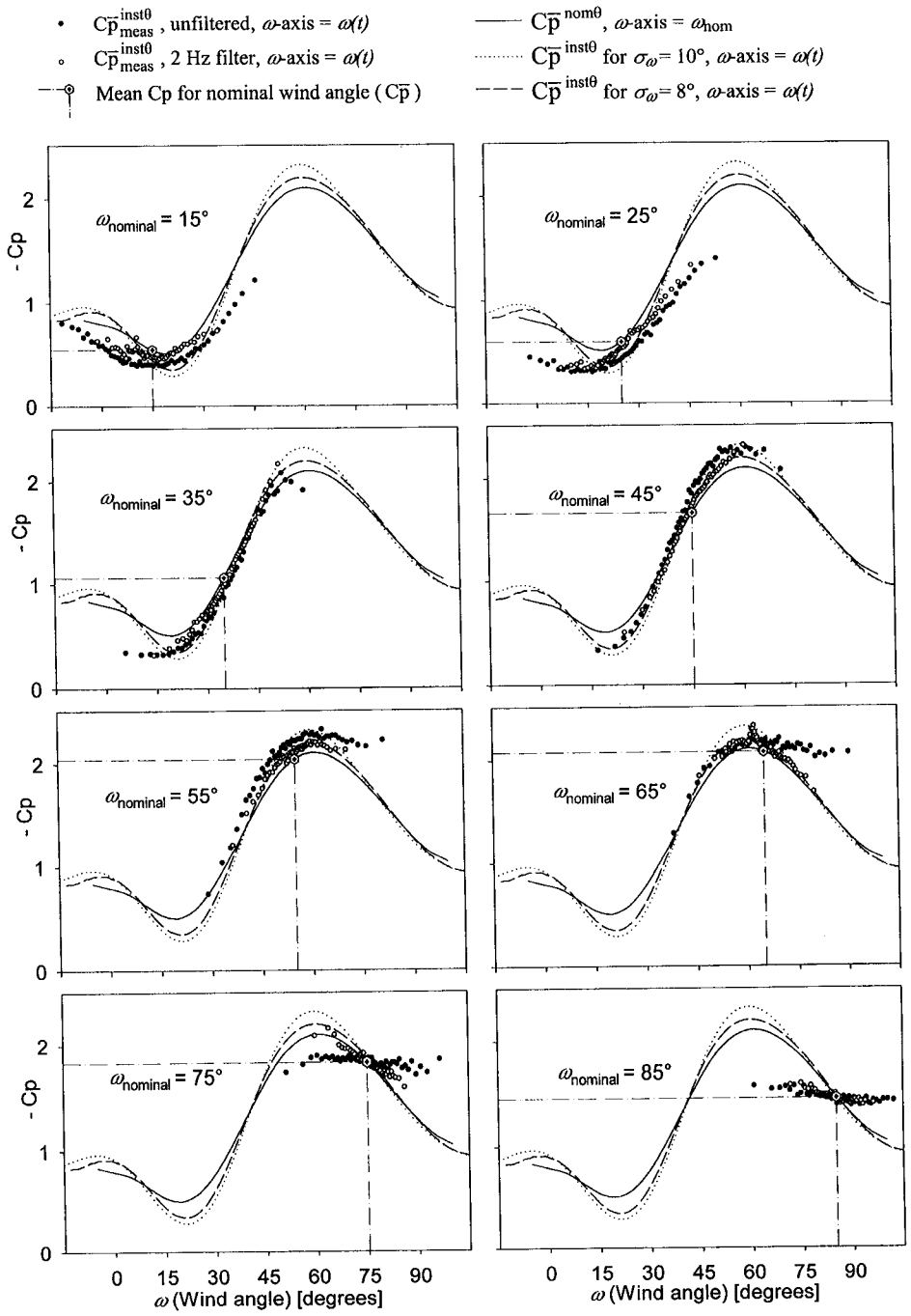

Fig. 9. Testing the quasi-steady assumption of wind angle dependence, tap #9.

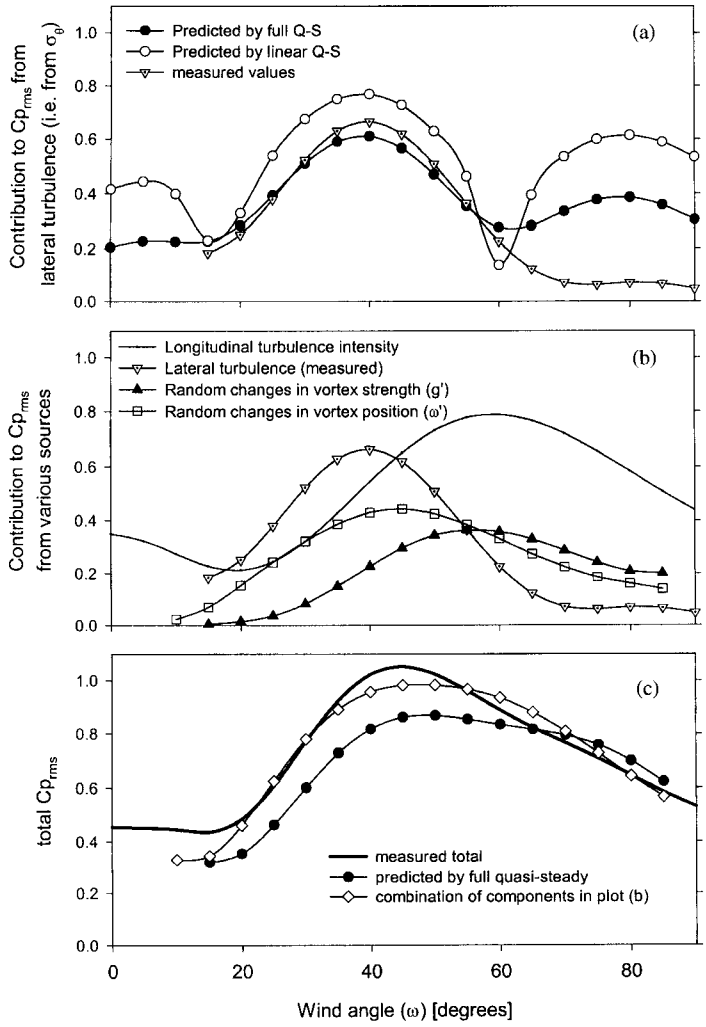

Fig. 10. (a–c) Components of $C_{p_{rms}}$ for tap #9.

where I_v (the lateral turbulence intensity) is commonly substituted for σ_θ [4,5]. This linear approximation is only useful when the value of a linear fit to $C_p(\theta)$ is valid over a range of around $\pm 2\sigma_\theta$, which is seldom the case, especially for most crucial wind directions, near pressure peaks. Note also that the linear approximation is much more effective if σ_θ is small. The value of σ_{C_p} from Eq. (13) is also depicted in Fig. 10a.

As might be expected from the results in Fig. 9, quasi-steady prediction agrees quite well with the measured values for $30^\circ < \omega < 60^\circ$, since the measured $C_{\tilde{p}}^{\text{inst}\theta}(\omega)$ follows the predicted $C_{\tilde{p}}^{\text{inst}\theta}(\omega)$ quite well in this region. And since the measured $C_{\tilde{p}}^{\text{inst}\theta}(\omega)$ does not follow the predicted curve when $\omega > 60^\circ$, but instead remains

due to instantaneous changes in wind direction (σ_θ), and the $C_{p_{\rm rms}}$ what would be attributed to σ_θ if a unique $C_{\bar{p}}^{{\rm inst}\theta}$ did actually exist. Finally, we will also examine the contribution to $C_{p_{\rm rms}}$ of the $g'(t)$ and ω' terms from Eq. (6), the effects of which are neglected in quasi-steady theory.

4.2.1. The quasi-steady $C_{p_{\rm rms}}$ equation

The rms value of any function $R = R(x_1, x_2, \ldots, x_n)$ can be estimated using the relation

$$\sigma_R^2 = \left(\overline{\frac{\partial R}{\partial x_1}}\sigma_{x_1}\right)^2 + \left(\overline{\frac{\partial R}{\partial x_2}}\sigma_{x_2}\right)^2 + \cdots \left(\overline{\frac{\partial R}{\partial x_n}}\sigma_{x_n}\right)^2. \tag{9}$$

If the turbulence intensity term from Eq. (2b) is re-introduced into Eq. (3), the quasi-steady equation can be written as

$$C_p^{\rm Q-S}(t, \theta) = \left(\frac{U_{\rm ref}(t)}{\bar{U}_{\rm ref}}\right)^2 \frac{C_{\bar{p}}(\theta)}{1 + I_U^2}. \tag{10}$$

Note again that the function $C_{\bar{p}}(\theta) \equiv C_{\bar{p}}^{{\rm inst}\theta}(\theta)$ is the most accurate function to use in the quasi-steady equation, since it yields $\overline{C_p(t, \theta(t) = \theta)} = C_{\bar{p}}^{{\rm inst}\theta}(\theta)$ and $\overline{C_p(t, \theta(t))} = C_{\bar{p}}^{{\rm nom}\theta}(\theta)$ in Eq. (10). This implies that $C_{\bar{p}}(\theta) = C_{\bar{p}}^{{\rm inst}\theta}(\theta)/(1 + I_U^2)$ should be used in the standard quasi-steady relation, Eq. (3).

Applying Eq. (9) into Eq. (10), where x_1 is the normalized velocity and $x_2 = C_p(\theta)$, gives

$$\sigma_{C_p(t)}^2(\theta) = \left(\frac{C_{\bar{p}}^{{\rm nom}\theta}(\theta)}{(1 + I_U^2)} 2I_U\right)^2 + \sigma_{C_{\bar{p}}(\theta)}^2 \quad \text{since } \sigma_{(U(t)/\bar{U})^2} = 2I_U. \tag{11}$$

The first term in Eq. (11) depends directly on the value of $C_{\bar{p}}^{{\rm nom}\theta}(\omega)$ and the turbulence intensity. The second term accounts for the effects of shifting wind direction, σ_θ, also refered to as lateral turbulence.

4.2.2. Calculating the contribution of lateral turbulence, σ_θ

Eq. (11) is also given in Ref. [7], as is a method of solving for the expected value of $C_{p_{\rm rms}}(\theta)$:

$$\begin{aligned}\sigma_{C_{\bar{p}}(\theta)}^2(\bar{\theta}) &= C_{p_{\rm rms}\_\theta}(\theta) = E[(C_{\bar{p}}^{{\rm inst}\theta}(\theta) - C_{\bar{p}}^{{\rm nom}\theta}(\bar{\theta}))^2] \\ &= \frac{1}{\sqrt{2\pi}\sigma_\theta}\int_{-\infty}^{\infty}\left(C_{\bar{p}}^{{\rm inst}\theta}(\theta) - C_{\bar{p}}^{{\rm nom}\theta}(\bar{\theta})\right)^2 \exp\left(-(\theta - \bar{\theta})/2\sigma_\theta\right)^2 {\rm d}\theta. \end{aligned} \tag{12}$$

If this integral is solved using the unique $C_{\bar{p}}^{{\rm inst}\theta}(\omega)$ curve, it provides the predicted $C_{p_{\rm rms}}$ contribution of σ_θ for the full quasi-steady evaluation. If instead the $C_{\bar{p}}^{{\rm inst}\theta}(\omega)$ data points shown in Fig. 9 are used in Eq. (12), then the actual contribution of σ_θ to σ_{Cp} is obtained. The results of both calculations are shown in Fig. 10a.

If instead the linear approximation (Eq. (8)) is used to calculate $\sigma_{C_{\bar{p}}(\theta)}$, the result is

$$\sigma_{C_{\bar{p}}(\theta)} = \left|\frac{\partial C_{\bar{p}}(\theta)}{\partial\theta}\right|\sigma_\theta, \tag{13}$$

data from taps beneath the conical vortices for certain wind directions has displayed a bi-modal distribution [5,31] which is not well represented by any of these models. It will be shown in the following section that the various shapes of the C_p pdf's beneath the conical vortices are largely due to instantaneous changes in the wind direction, which are well predicted by quasi-steady theory if Eq. (3) is evaluated fully.

4.3.1. Calculating the pdf

If both the $(U/\bar{U})^2$ and $C_{\bar{p}}(\theta)$ terms in Eq. (3) are linearized, then the pdf for $C_p(t)$ becomes Gaussian, since the pdf for $\theta(t)$ and $U(t)$ are Gaussian [5]. As mentioned above, wind pressures on buildings rarely are Gaussian, so this approximation cannot be considered valid.[2]

The pdf of $C_p^{\mathrm{Q-S}}(t)$ can be evaluated fully from Eq. (3) using the general principal that the probability distribution of a function $z = x \cdot y$ can be calculated using the convolution integral

$$f_z(z)\,\mathrm{d}z = \int_{-\infty}^{\infty} f_y(z/x) f_x(x)\,\mathrm{d}A.$$

This can be evaluated discretely as

$$f_z(z_i) = \sum_{x_n=x_{\min}}^{x_n=x_{\max}} f_y(z_i/x_n) f_x(x_n) \ln\left(\frac{x_n + \Delta x}{x_n - \Delta x}\right),$$

where $\Delta x = x_{i+1} - x_i$, and $f_x(x) = 0$ for $x < x_{\min}$ and $x > x_{\max}$. Applying this to Eq. (3) for tap #9 gives

$$f_{C_p^{\mathrm{Q-S}}}(C_{p_i}^{\mathrm{Q-S}}) = \sum_{C_{\bar{p}}(\theta)_n=-2.3}^{C_{\bar{p}}(\theta)_n=-0.4} f_{(U/\bar{U})^2}(C_{p_i}^{\mathrm{Q-S}}/C_{\bar{p}}(\theta)_n) f_{C_{\bar{p}}(\theta)}(C_{\bar{p}}(\theta)_n) \times \ln\left(\frac{C_{\bar{p}}(\theta)_n + \Delta C_{\bar{p}}(\theta)}{C_{\bar{p}}(\theta)_n - \Delta C_{\bar{p}}(\theta)}\right), \tag{14}$$

so that, for example, the probability that $C_p^{\mathrm{Q-S}} = -1$ is the sum of the weighted probabilities that when $C_p(\theta) = -1$, $(U/\bar{U})^2 = 1$, and when $C_p(\theta) = -1.5$, $(U/\bar{U})^2 = 0.67$, etc.

The pdf's $f_{(U/\bar{U})^2}$ and $f_{C_{\bar{p}}(\theta)}$ can be calculated from the Gaussian pdf's of $U(t)$ and $\theta(t)$. In general, if x is a function of ξ, and ξ has a known pdf $f_\xi(\xi)$, then

$$f_x(x) = \frac{f_\xi(\xi_1)}{|x'(\xi_1)|} + \frac{f_\xi(\xi_2)}{|x'(\xi_2)|} + \cdots + \frac{f_\xi(\xi_n)}{|x'(\xi_n)|}, \tag{15}$$

where the x' is the partial derivative of x with respect to ξ, and n is the number of different roots for a given value of x. Applying Eq. (15) to the function $C_{\bar{p}}^{\mathrm{inst}\theta}$ for $\sigma_\theta = 10°$ from Fig. (9) resulted in anywhere from 2–4 roots. For example, since $C_{\bar{p}}^{\mathrm{inst}\theta} = -2$ for both $\theta = 72°$ and 49°, $f_{C_{\bar{p}}(\theta)}(-2)$ would have two roots, so that the probability that $C_p = -2$ is the sum of the weighted probabilities that $\theta = 72°$ or 49°.

[2] Holmes [32] has shown clearly how the $(U/\bar{U})^2$ term is expected to produce a skewed distribution, so that it is perhaps worth asking why any of a building's pressure taps would register a Gaussian C_p pdf.

fairly constant for any instantaneous wind angle, the quasi-steady theory (both the linear estimate and the full integral) actually overpredicts $C_{p_{\text{rms}}}$ due to σ_θ at these wind angles.

The linear model also underpredicts $C_{p_{\text{rms}\_\theta}}$ at the peaks ($\omega = 25°$ and 60°), and overpredicts $C_{p_{\text{rms}\_\theta}}$ when the $C_p(\theta)$ slope is high. These errors are paradoxically reduced if the differential in Eq. (13) is performed crudely, with large $\Delta\omega$ steps both in the derivative and between the location where it is evaluated.

4.2.3. *Contributions to σ_{C_p} neglected by quasi-steady theory*

Applying Eq. (9) into Eq. (6) yields two additional terms:

$$\sigma^2_{C_p}(\theta) = \left(C_{p_{\text{rms}\_\text{TI}}}\right)^2 + \left(C_{p_{\text{rms}\_\theta}}\right)^2 + \left(C_{p_{\text{rms}\_g'}}\right)^2 + \left(C_{p_{\text{rms}\_\omega'}}\right)^2,$$

where the first two terms are the turbulence intensity and wind direction shift (lateral turbulence) terms from Eq. (11), and the last two terms are calculated as

$$C_{p_{\text{rms}\_g'}}(\omega) = (1 + I_U^2)\left(\frac{\bar{U}_{\text{M}}(\omega)}{\bar{U}_{\text{ref}}}\right)^2 \sin^2(\alpha) g(\omega)\eta(\omega)\sigma_{g'},$$

$$C_{p_{\text{rms}\_\omega'}}(\omega) = (1 + I_U^2)(C_{p_{\text{S}}}(\omega) - C_{p_{\text{a}}})\frac{\partial\eta(\omega)}{\partial\omega}\omega\sigma_{\omega'}.$$

(Note that the techniques to be described in Section 4.3.1 can be used to generate a more accurate prediction of $C_{p_{\text{rms}\_\omega'}}$ from $f_{\omega'}(\omega')$ and $\eta(\omega)$ than the above linear approximation.)

$C_{p_{\text{rms}\_g'}}$ accounts for random changes in the vortex quality or strength, while $C_{p_{\text{rms}\_\omega'}}$ accounts for random changes in the vortex position (recall Fig. 6). These two terms are shown as functions of ω_{nom} in Fig. 10(b), along with the turbulence intensity and wind direction shift terms. The values of $\sigma_{g'}$ and $\sigma_{\omega'}$ have been estimated at 0.45 and 0.33, respectively. Fig. 10(c) shows how the omission of these terms compensates for the quasi-steady theory's over prediction of the effects of lateral turbulence for some wind angles (e.g. near 70°), but leads to underprediction at the crucial worst case wind angles (near 45°).

4.3. *Probability distribution functions*

While matching the predicted and measured rms C_p values is an important aspect of quasi-steady theory validation, a comparison of the probability distribution function (pdf) of $C_p^{\text{Q-S}}(t)$ and $C_p(t)$ provides a comprehensive picture of the accuracy of the quasi-steady model. This is particularly important for the prediction of peak suction events, since the pdf's of surface pressures on all faces of a square cylinder but the front are not normal (Gaussian) [27,28]. Studies have also shown that the skewness and kurtosis (flatness) varies greatly with the position on the building [29], so that a knowledge of $C_{p_{\text{mean}}}$ ($C_{\bar{p}}$) and $C_{p_{\text{rms}}}$ (σ_{C_p}) is not adequate to predict the expected peak suction.

Weibull, gamma, and log-normal distributions have all been used with reasonable success to represent C_p pdf's for different building pressure time series [30]. However,

those calculated from the predicted $C_{\bar{p}}^{\text{inst}\theta}$ curves for $\omega < 50°$, but do not agree for $\omega > 60°$. In particular, the pdf for $\omega_{\text{nom}} = 85°$ appears as a narrow spike at $C_p(\theta) = 1.5$, because $C_{\bar{p}_{\text{meas}}}^{\text{inst}\theta}$ is almost independent of ω for this wind angle.

Eq. (15) can also be used to derive $f_{(U/\bar{U})^2}$ from f_U. In this case, there is only one root, so that

$$f_{(U/\bar{U})^2} = \frac{\bar{U}^2}{2}\frac{f_U(U)}{U} = \frac{\bar{U}^2}{2U\sigma_U\sqrt{2\pi}}\exp\left(\frac{-(U-\bar{U})^2}{2\sigma_U^2}\right).$$

Combining $f_{(U/\bar{U})^2}$ with the $f_{C_{\bar{p}}(\theta)}$ curves in Fig. 11 as described in Eq. (14) produces the pdf's shown in Fig. 12. These are compared to histograms of the experimental data. Note that $C_{\bar{p}}(\theta) = C_{\bar{p}}^{\text{inst}\theta}(\theta)/(1 + I_U^2)$ was used to determine $f_{C_{\bar{p}}(\theta)}$, as advised in Eq. (10). Also shown in Fig. 12 are selected Gaussian pdf's calculated using the mean and rms from the experimental data, as well as selected C_p pdf's calculated from the measured $C_{\bar{p}_{\text{meas}}}^{\text{inst}\theta}(\theta)$ that were shown in Fig. 11. Fig. 12(b) presents the same data on a semilog scale, which allows a better look at the tails of the pdf's.

4.3.2. Quasi-steady inaccuracy near $C_{\bar{p}} = 0$

Eq. (3) does not allow the possibility that $C_p(t) > 0$ for tap #9, since $C_{\bar{p}}(\theta)$ is never > 0. The data indicate, however, that $C_p(t)$ does occasionally become positive, especially when $|C_{\bar{p}}(\theta)|$ becomes small, such as for $\omega < 30°$. This is at least partly due to the nature of the static pressure fluctuations in the wind tunnel, which have been studied in more detail in Ref. [9].

Static pressure time series were simultaneously measured during this experiment using pressure taps on the walls of the tunnel, as well as pitot tubes at model height and 1.5 m above the tunnel floor. These measurements indicate the presence of static pressure fluctuations at these various locations which were correlated at low frequencies, but which were not correlated to the flow velocity. Applying this knowledge to the definition of $C_p(t)$ gives

$$\begin{aligned} C_{p_{\text{M}}}(t) &= \frac{p_{\text{M}}^{\text{static}}(t) - p_{\text{ref}}^{\text{static}}(t)}{\frac{1}{2}\rho\left(\overline{U_{\text{ref}}}\right)^2} + \frac{p_{\text{M}}^{\text{static-random}}(t) - p_{\text{ref}}^{\text{static-random}}(t)}{\frac{1}{2}\rho\left(\overline{U_{\text{ref}}}\right)^2} \\ &= C_{p_{\text{M}}}^{\text{Q-S}}(t) + C_{p_{\text{M}}}^{\text{s-r}}(t), \end{aligned}$$

so that the experimental values have a random noise component is added to the quasi-steady C_p measurement. This random noise component, $C_{p_{\text{M}}}^{\text{s-r}}(t)$, was measured experimentally by comparing the static pressure fluctuations between the various locations mentioned above. It has a normal distribution with $C_{p_{\text{M}}}^{\text{s-r}}(t) = 0$ and $\sigma_{Cp^{\text{s-r}}} = 0.12$ (see Fig. 13). As a result, it has little influence on larger $|C_p|$ values, but will change the pdf for small $|C_p|$ values. The pdf changes can be calculated with the convolution integral

$$f_{C_p}(C_p) = \int_{C_{p\min}^{\text{Q-S}}}^{C_{p\max}^{\text{Q-S}}} f_{Cp^{\text{s-r}}}(C_p - C_p^{\text{Q-S}}) f_{C_p^{\text{Q-S}}}(C_p^{\text{Q-S}})\,\mathrm{d}C_p^{\text{Q-S}}. \tag{16}$$

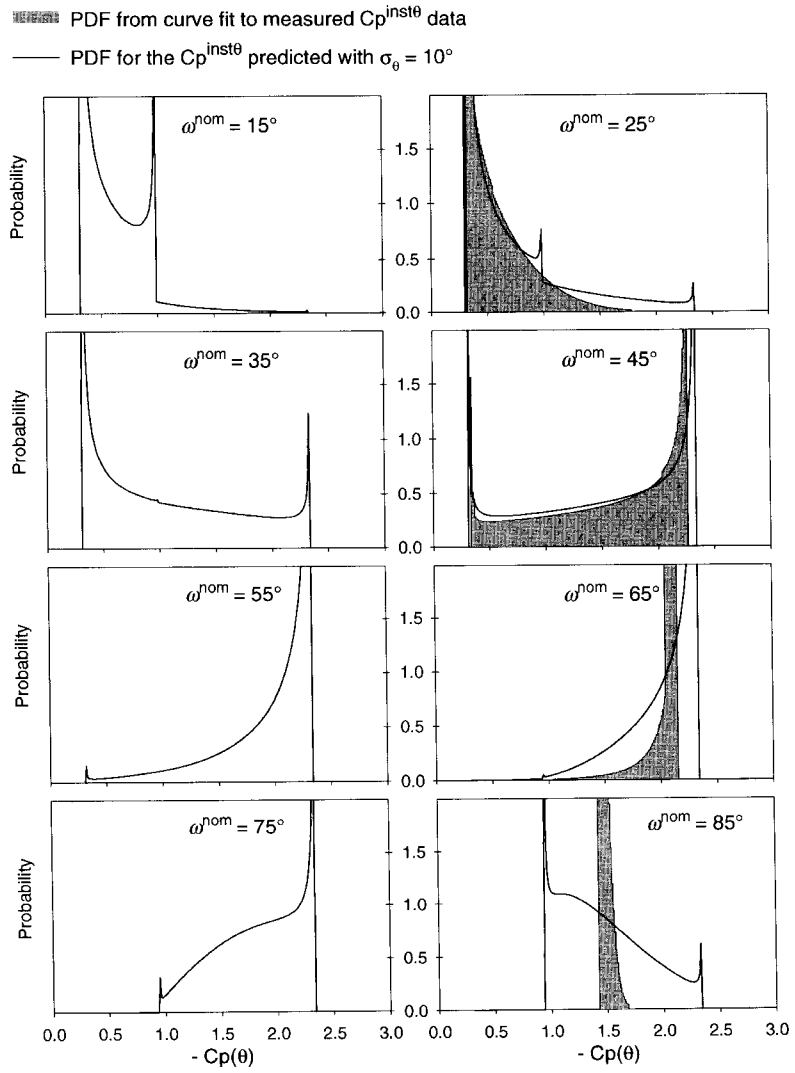

Fig. 11. Probability distributions of $C_p(\theta)$ at tap #9 for various nominal wind directions.

(This is the procedure that was used to derive the $f_{C_p}(C_p)$ pdf in Fig. 8.) Fig. 11 shows the $f_{C_{\tilde{p}}(\theta)}$ curves for tap #9 that were calculated for various nominal wind angles using a Gaussian pdf with $\sigma_\theta = 10°$ for $f_\theta(\theta)$. The sharp peaks are the result of small $C'_p(\theta)$ values at the various $C_{\tilde{p}}^{\text{inst}\theta}$ maxima and minima. Of particular interest is $f_{C_{\tilde{p}}(\theta)}$ for $\omega_{\text{nom}} = 45°$, which has peaks at $C_p = -0.3$ and -2.35. This is essentially what causes the bimodal behaviour of f_{Cp}; this will be discussed further later in this paper.

Also shown are selected $f_{C_{\tilde{p}}(\theta)}$ curves derived from applying Eq. (15) to curve fits of the measured $C_{\tilde{p}_{\text{meas}}}^{\text{inst}\theta}(\theta)$ values of Fig. 9. As expected, these pdf's agree fairly well with

histograms than the predictions made with the measured $C^{\text{inst}\theta}_{\bar{p}_{\text{meas}}}$ curves. This could also have been anticipated from Fig. 10, where the quasi-steady over-prediction of $C_{p_{\text{rms}\_\theta}}$ compensates for the absence of a $C_{p_{\text{rms}\_\omega'}}$ term.

The vortex motion which is expressed by the ω' term is not included in the quasi-steady model. As a result, the quasi-steady theory is bound to underestimate the frequency of peak suction events, since these events are tied to the presence of the vortex core above the tap. In the quasi-steady model, this can only occur during a shift in wind direction, while in fact random core motion can move the vortex over the tap for any wind direction.

For $\omega(t) < 30^\circ$ and $\omega(t) > 70^\circ$, this under-prediction is compensated for in quasi-steady theory by the over-prediction of the effects of σ_θ by the use of $C^{\text{inst}\theta}_{\bar{p}}$ curve in Eq. (10), which incorrectly assumes that a shift in instantaneous wind direction to $\omega(t) = 65^\circ$ produces the same suction regardless of ω_{nom}.

5. Conclusions

Since the quasi-steady theory is based in part on Bernoulli's equation, it would not be expected to predict C_p values well under the separated flow around a rooftop conical vortex. However, because the vortex transfers to the roof surface the effects of flow speed and direction changes above the separated flow zone, there is some reason to believe that the quasi-steady theory could produce reasonably accurate results when applied fully. In fact, a full quasi-steady evaluation is able to reproduce the skewed C_p probability distribution function (pdf) shapes reasonably well, including the bi-modal pdf which is observed at cornering wind directions for some taps near the vortex.

However, the results of this study caution against the use of quasi-steady theory to predict peak and rms pressure coefficients near the roof-top conical vortices. For certain taps at certain wind angles, the quasi-steady theory can produce accurate predictions for these fluctuating pressure coefficients. However, this accuracy is achieved through a fortuitous combination of incorrect assumptions which offset each other's effects.

The basic assumption of quasi-steady theory as applied fully to the pressures near the vortex is that any change in wind direction will result in a known change in vortex position and strength. This is demonstrated in this study to be the case only for mean wind angles of $35^\circ < \omega < 55^\circ$. At other mean wind angles, momentary changes in wind direction have much less effect on the vortex than quasi-steady theory assumes. This essentially means that quasi-steady theory overpredicts the effects of lateral turbulence on taps near the conical vortex for mean angles above 60° or below 30°.

Quasi-steady theory neglects the effects of random changes in vortex strength and position. These changes are described in this study by the terms g' and ω' respectively. The effects of these terms on $C_{p_{\text{rms}}}$ at a tap near the roof corner are quantified in this study, and are seen to be comparable to the effects of lateral turbulence.

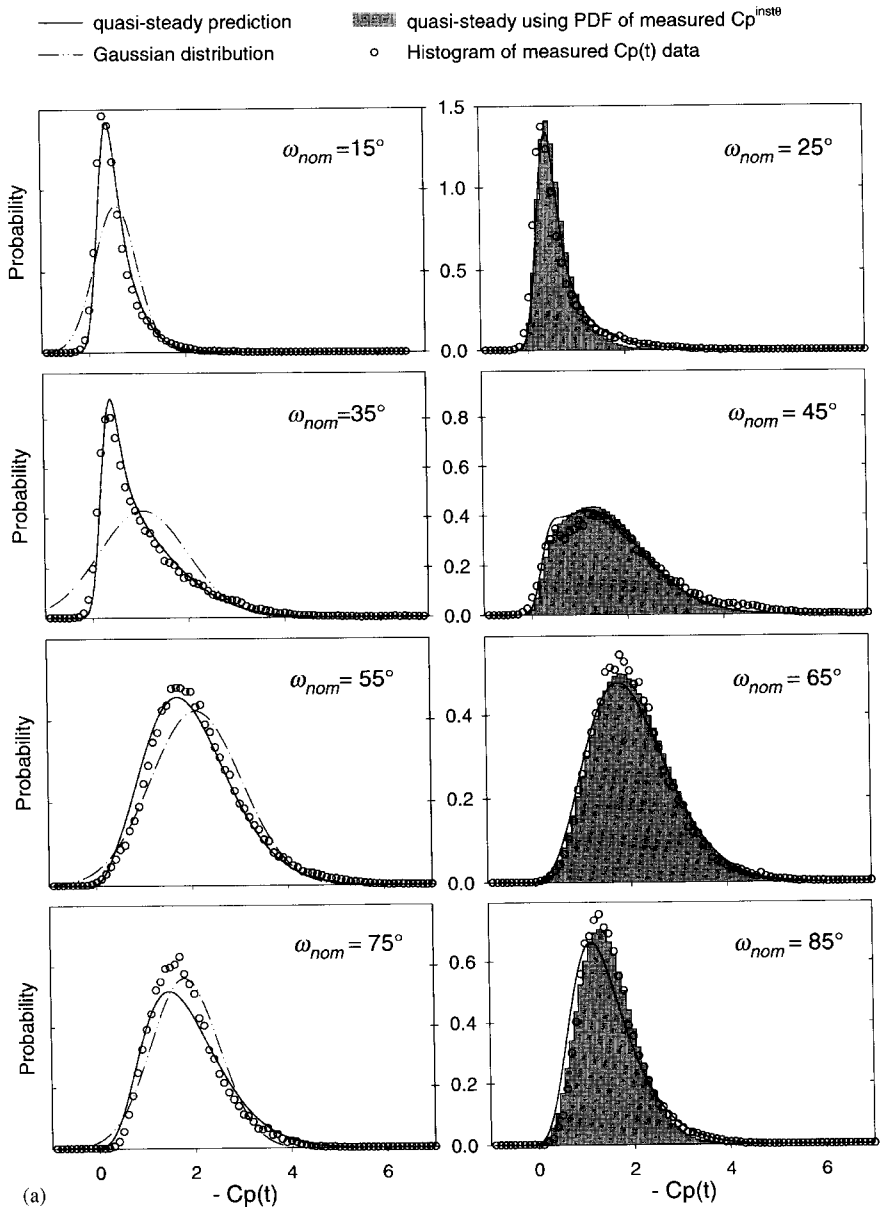

Fig. 12. (a) Probability distributions of $C_p(t)$ at tap #9 for various nominal wind directions (linear plots).

This additional calculation was performed for all the plots in Fig. 12, and is shown to account for the existence of C_p values greater than 0. An example of the changes to the pdf is shown in Fig. 13(b) for $\omega_{\text{nom}} = 45°$.

[6] I. Calderone, J.C.K. Cheung, W.H. Melbourne, The full-scale significance on glass cladding panels, of data obtained from wind tunnel measurements of pressure fluctuations on building cladding, J. Wind Eng. Ind. Aerodyn. 53 (1994) 247–259.
[7] P.J. Richards, R.P. Hoxey, B.S. Wanigaratne, The effect of directional variations on the observed mean and rms pressure coefficients, J. Wind Eng. Ind. Aerodyn. 54/55 (1995) 359–367.
[8] C.W. Letchford, R. Marwood, On the influence of v & w component turbulence on roof pressures beneath conical vortices, J. Wind Eng. Ind. Aerodyn. 69–71 (1997) 567–577.
[9] D. Banks, The Suction Induced by Conical Vortices on Low-Rise Buildings with Flat Roofs, Ph.D. dissertation, Civil Engineering Department, Colorado State University, Fort Collins, CO, 2000.
[10] D. Banks, R.N. Meroney, P.P. Sarkar, Z. Zhao, F. Wu, Flow visualization of conical vortices on flat roofs with simultaneous surface pressure measurement, J. Wind Eng. Ind. Aerodyn. 84 (2000) 65–85.
[11] B.B. Yeatts, K.C. Mehta, D.A. Smith, Field experiments for wind effects on low buildings, 9th International Conference on Wind Engineering, New Delhi, India, 1995.
[12] H.J. Ham, B. Bienkiewicz, Wind tunnel simulation of TTU flow and building roof pressure, J. Wind Eng. Ind. Aerodyn. 77,78 (1998) 119–133.
[13] D. Banks, and R.N. Meroney, A model of roof-top surface pressures produced by conical vortices: evaluation and implications, Wind and Structures, 2000, accepted for publication.
[14] D. Banks, R.N. Meroney, A model of roof-top surface pressure dependence upon local flow parameters, Wind Engineering into the 21st Century, the 10th International Conference on Wind Engineering, Copenhagen, Denmark, 1999.
[15] D. Banks, R.N. Meroney, A model of roof-top surface pressures produced by conical vortices: model development, Wind and Structures, 2000, accepted for publication.
[16] Q.S. Li, W.H. Melbourne, An experimental investigation of the effects of free-stream turbulence on streamwise surface pressures in separated and reattaching flows, J. Wind Eng. Ind Aerodyn. 54/55 (1995) 313–323.
[17] W.H. Melbourne, Turbulence and the Leading Edge Phenomena, J. Wind Eng. Ind. Aerodyn. 49 (1993) 45–64.
[18] C.P.W. Geurts, Full-scale and wind-tunnel measurements of the wind and wind-induced pressures over suburban terrain, J. Wind Eng. Ind. Aerodyn. 64 (1996) 89–100.
[19] C.P.W. Geurts, H.S. Rutten, J.A. Wisse, Spectral characteristics of wind induced pressures on a full scale building in suburban terrain, J. Wind Eng. Ind. Aerodyn. 69–71 (1997) 609–618.
[20] R. Sankaran, E.D. Jancauskas, Measurements of cross-correlation in separated flows around bluff cylinders, J. Wind Eng. Ind. Aerodyn. 49 (1993) 279–288.
[21] H. Kawai, Pressure fluctuations on square prisms – Applicability of strip and quasi-steady theories, J. Wind Eng. Ind. Aerodyn. 13 (1983) 197–208.
[22] H. Kawai, G. Nishimura, Characteristics of fluctuating suction and conical vortices on a flat roof in oblique flow, J. Wind Eng. Ind. Aerodyn. 60 (1996) 211–225.
[23] A. Papoulis, Probability, Random Variables, and Stochastic Processes, McGraw-Hill Book company, New York, 1984.
[24] J. Maier-Erbacher, E.J. Plate, Measurement of velocity near and pressure on a cylindrical tower located on irregular terrain, J. Wind Eng. Ind. Aerodyn. 38 (1991) 167–184.
[25] R.P. Hoxey, P.J. Richards, G.M. Richardson, A.P. Robertson, J.L. Short, The Silsoe structures building: the completed experiment part 2, 9th International Conference on Wind Engineering, New Delhi, India, 1995.
[26] R.P. Hoxey, A.P. Robertson, Pressure coefficients for low-rise building envelopes derived from full-scale experiments, J. Wind Eng. Ind. Aerodyn. 53 (1994) 283–297.
[27] J.L.D. Ribeiro, J. Blessmann, Probability distribution of forces and pressures on a square cylinder, J. Wind Eng. Ind. Aerodyn. 41–44 (1992) 813–824.
[28] J.A. Peterka, J.E. Cermak, Wind pressures on Buildings – Probability Densities, J. Struct. Div. ASCE 101 (1975) 1255–1267.
[29] T. Stathopoulos, pdf of Wind Pressures on Low-Rise Buildings, J. Struct. Div. ASCE 106 (1980) 973–990.

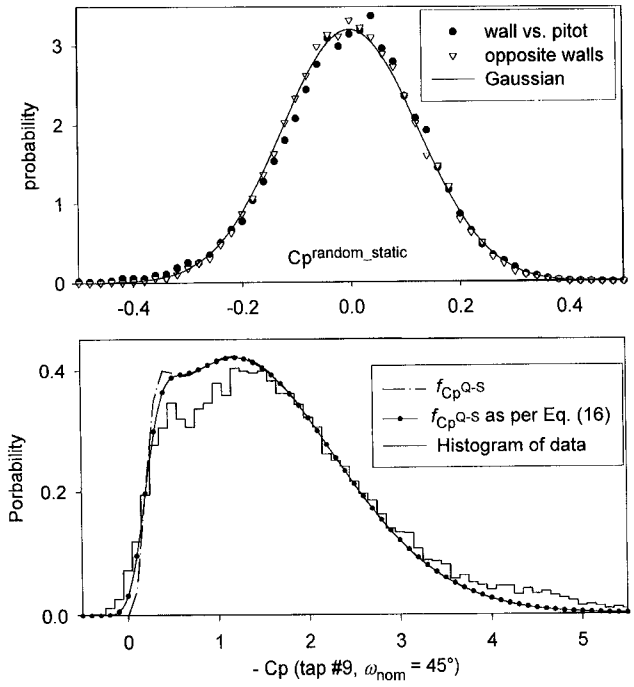

Fig. 13. Effect of Random static pressure fluctuations on pdf of C_p (tap #9, for nominal wind direction = 45°).

$\omega_{nom} = 45°$. When $\omega(t) < 20°$, tap #9 is generally beyond the reattachment point, and so has $C_p \approx C_{pa}$. For $\omega(t) > 30°$, the tap is typically beneath the zone of flow separation, and lower C_p's are evident. The bimodal distribution is the result of the tap being intermittently inside the separated flow zone, where a C_p pdf like that for $\omega_{nom} = 65°$ dominates, and outside the separated flow, where a C_p pdf like that for $\omega_{nom} = 25°$ dominates. Another way to think of the bimodal distribution is that it is the half-way point of the histogram transition from having a peak at $C_p = -0.4$ and $C_p = -2$. This is perhaps more evident in the log plots, as the negative tail rises up as ω_{nom} increases.

The change in the position of the reattachment and the vortex core is largely due to the change in the instantaneous wind angle. This is well modeled by the quasi-steady theory, especially for $\omega(t) < 50°$, as is evident in Figs. 9 and 11. The result is that the quasi-steady predictions of $f_{C_{\tilde{p}}(\theta)}$ match the measured histograms well for $\omega(t) < 50°$, as seen in Fig. 12. However, the quasi-steady prediction of $f_{C_{\tilde{p}}(t)}$ for $\omega(t) > 60°$ is much less accurate, as was seen in Fig. 11. This has surprisingly little effect on the overall pdf, which on the linear plot (Fig. 12(a)) matches the data fairly well. This is because of the dominance of the $f_{(U/\bar{U})^2}$ distribution, which might be expected in this region, given the dominance of $C_{p_{rms\_TI}}$ seen in Fig. 10 for these wind angles.

When viewed on a log scale in Fig. 12(b), the quasi-steady predictions made using the unique predicted $C_{\tilde{p}}^{inst\theta}$ curve actually show a better agreement with the data

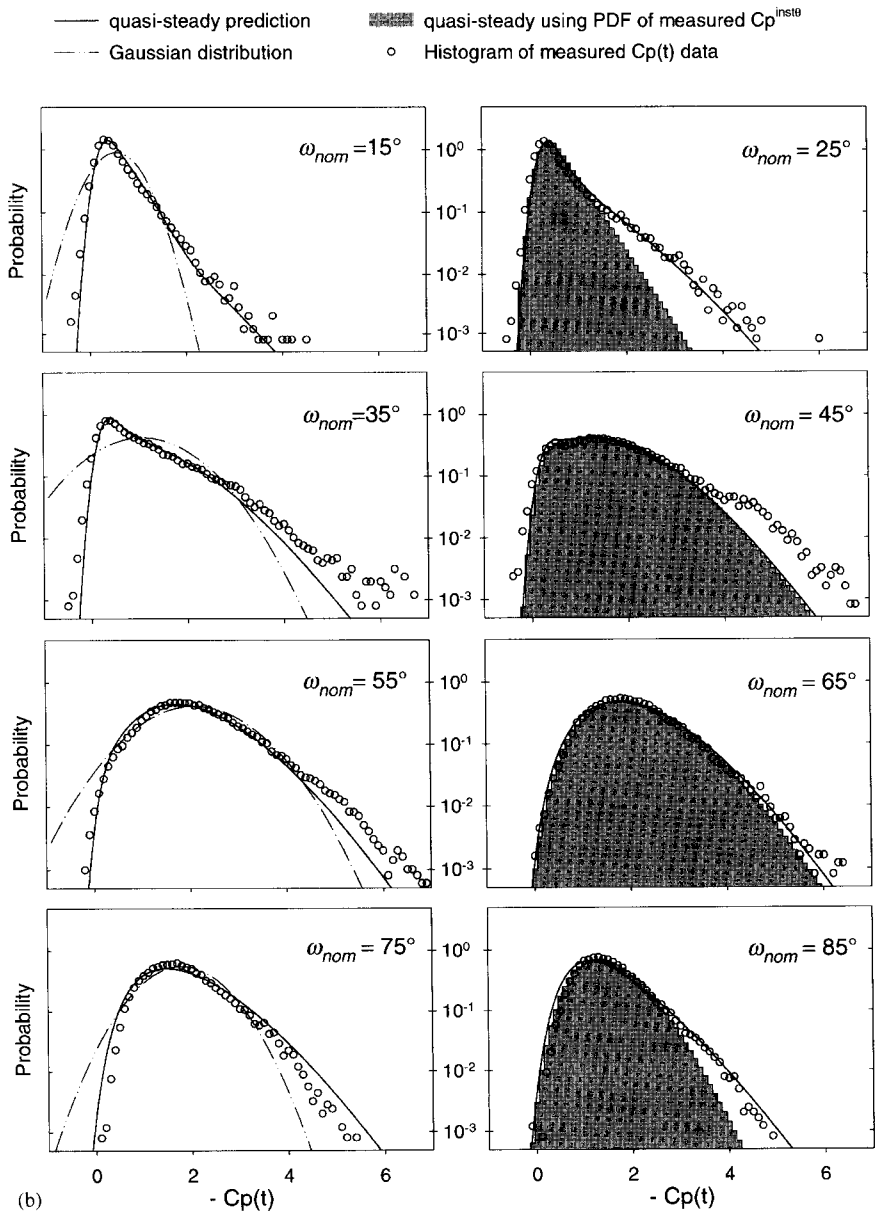

Fig. 12. (b) Probability distributions of $C_p(t)$ at tap #9 for various nominal wind directions (log plots).

4.3.3. *Discussion of pdf shape*

Both the predicted and the measured histogram of $C_p(t)$ for tap #9 when $\omega_{\text{nom}} = 45°$ shows two peaks, an abrupt one at $C_p = 0.5$ and the more gradual peak at $C_p = 1.2$ (see Fig. 13). This is the result of the extreme bimodal nature of $f_{C_{\tilde{p}}(\theta)}$ for

The net effect is that when the quasi-steady theory is used to predict a C_p pdf for a tap near the vortex, it produces a surprisingly good match to the data for mean wind angles less than 30° or greater than 60°. This is because the overprediction of the influence of lateral turbulence has compensated for the neglected terms. However, in the crucial range of $30° < \omega < 60°$, where the worst case suctions are likely to occur, the lateral turbulence is fairly accurately described by the quasi-steady model. The net effect here then is the underprediction of the worst peak suctions.

Finally, we would like to make the following suggestions for further study of the application of the quasi-steady model:

- The use of C_p pdf's rather than $C_{p_{\text{rms}}}$ or $C_{p^{\text{v}}}$ provides much more insight into the nature of the data and of the quasi-steady model's predictions.
- Since the basic quasi-steady assumption is seen to be increasingly inaccurate as ω approaches 90° or 0° (flow normal to a wall), quasi-steady theory is not expected to properly describe the suction beneath bubble separation, where the relative influence of the g' term is expected to be at its greatest.
- This study was performed in a single boundary layer, which was designed to simulate conditions at the TTU WERFL site. In a different boundary layer, the ratio of the effects of I_{U}, σ_θ, g' and ω' can be expected to change, which further underlines the danger of using a theory which inaccurately characterizes their relative influences on $C_p(t)$.
- The parameters which control g' and ω' are not known at this time. It is conceivable that very small scale turbulence (of the order of the shear layer thickness) influence this random vortex change. Such small and rapid fluctuations may best be investigated at full scale.

Acknowledgements

The contribution of Dr. David E. Neff in implementing the experimental facilities at CSU is gratefully acknowledged. This work was supported by the US National Science Foundation through the CSU/TTU Cooperative Program in Wind Engineering, Grant No. CMS-9411147.

References

[1] N.J. Cook, The designer's guide to wind loading of building structures, part 2: static structures, Building Research Establishment Report, Garston, UK, 1990.
[2] P.J. Saathoff, W.H. Melbourne, The generation of peak pressures in separated/ reattaching flows, J. Wind Eng. Ind. Aerodyn. 32 (1989) 121–134.
[3] Y. Uematsu, N. Isyumov, Peak gust pressures acting on the roof and wall edges of a low-rise building, J. Wind Eng. Ind. Aerodyn. 77,78 (1998) 217–231.
[4] H.W. Tieleman, M.R. Hajj, Pressures on a flat Roof-application of Quasi-Steady Theory, 1995 ASCE Engineering Mechanics Conference, Boulder, CO, 1995.
[5] C.W. Letchford, R.E. Iverson, J.R. McDonald, The application of the Quasi-Steady theory to full scale measurements on the Texas Tech Building, J. Wind Eng. Ind. Aerodyn. 48 (1993) 111–132.

At $\omega_{\text{nom}} = 75°$, even the 2 Hz filter fails to keep the measured data on the predicted $C_{\bar{p}}^{\text{inst}\theta}$ line, and at $\omega_{\text{nom}} = 85°$, the behaviour is completely inconsistent with that expected by quasi-steady theory. We believe that this is because momentary wind direction excursions to $\omega < 75°$ fail to re-establish the consistent conical vortex needed to attain the kind of mean suction seen for $\omega_{\text{nom}} = 60°$.

The general picture of the flow mechanism under the separated flow along the leading edge provided by these observations is one in which the flow structure exhibits a kind of hysteresis, where the value of $C_{\bar{p}_{\text{meas}}}^{\text{inst}\theta}$ is dependent upon the direction in which the wind has shifted; $C_{\bar{p}_{\text{meas}}}^{\text{inst}\theta}$ (45°) is quite different for $\omega_{\text{nom}} = 25°$ and $\omega_{\text{nom}} = 65°$. This hysteresis can be reduced or eliminated in some cases by low-pass filtering the data, since a wind direction change of long enough duration will permit the transition from separation bubble to conical vortex to take place. However, the cutoff frequency needed for such filtering to be effective is extremely low ($T \sim 25$ s at full scale), so that the quasi-steady theory is not expected to offer a reliable estimate of 3 s gust loads except when $35° < \omega_{\text{nom}} < 55°$. As will be shown in the next section, other factors not considered in Eqs. (2a) and (2b) make the quasi-steady theory unreliable for predicted pressure fluctuations even for these mean wind directions.

4.2. Part 2: Rms pressures

One of the principal uses of the quasi-steady theory is to predict the surface pressure fluctuations ($C_{p_{\text{rms}}}(\theta)$, also written as $\sigma_{C_p}(\theta)$) based on flow velocity fluctuations. The underprediction of $C_{p_{\text{rms}}}$ is also one of the more commonly cited examples of the failure of quasi-steady theory [5,24]. Studies which rejected the use of the quasi-steady theory in zones of flow separation generally used a linear estimate for $C_{\bar{p}}(\theta)$ in Eq. (3):

$$C_{\bar{p}}(\theta) = C_{\bar{p}}(\bar{\theta}) + (\theta - \bar{\theta}) \frac{\partial C_{\bar{p}}(\bar{\theta})}{\partial \theta}. \tag{8}$$

This linear quasi-steady model is known to fail to adequately predict fluctuating pressures at the stagnation point on a circular tower [24]. As noted by Hoxey [25], the failure of the linear quasi-steady model to adequately predict measured σ_{Cp} values is largely attributable to the oversimplification in Eq. (8), and good σ_{Cp} agreement has been illustrated on windward facing taps and in separated flow zones when Eq. (3) is evaluated fully [26].

However, Section 4.1 has shown that the third quasi-steady assumption (that a change in $\theta(t)$ leads to a change in the expected value of $C_p(t)$ based on the $C_{\bar{p}}^{\text{inst}\theta}$ curve) is often incorrect near the roof top vortices, so that neither the full nor a linear quasi-steady models would be expected to correctly predict $C_{p_{\text{rms}}}$. For example, for $\omega_{\text{nom}} = 75°$, from Fig. 9 we see that ω has essentially no effect on the true expected value of C_p, so that a more accurate evaluation of $C_{\bar{p}}(\theta)$ in Eq. (3), will not improve the representation of what is actually happening.

To appreciate how quasi-steady theory sometimes matches the experimentally measured σ_{Cp} values in spite of this, we will examine both the true measured $C_{p_{\text{rms}}}$

[30] N. Hosoya, J.E. Cermak, J.A. Peterka, Probabilistic analysis of area-averaged pressures on model TTU building, 8th US National Conference on Wind Engineering, Baltimore, MD, 1997.
[31] L.S. Cochran, Wind tunnel modelling of low-rise structures, Ph.D., Civil Engineering, Colorado State University, Fort Collins, CO, 1992.
[32] J.D. Holmes, Non-Gaussian characteristics of wind pressure fluctuations, J. Wind Eng. Ind. Aerodyn. 7 (1981) 103–108.